Probing molecular layers with low-energy electrons

Tebyani, A.

5

Critical Role of Electronic States above the Vacuum Level in Photo-Electron and Secondary-Electron Emission in Few-Monolayer Pentacene Films *

Abstract

Electron states above the vacuum level are known to play an important role in secondary electron processes, such as photo-electron emission and secondary electron emission, where they act as “final” (or better: “intermediate”) states from which an electron is emitted to the vacuum. However, despite their relevance, these states are typically not well-known, nor independently investigated, mostly due to a lack of proper spectroscopic techniques. Here, we present a spectroscopy study on crystalline pentacene, used as a model system to investigate the influence of these states on secondary electron processes. Using low-energy electron (LEE) spectroscopy, we first gauge the spectrum of such states in few-monolayer pentacene films. We subsequently relate these states to photo-electron and secondary electron emission. Specifically, photo-emission experiments (Hg lamp) show a decrease of intensity with each additional pentacene layer grown. Given an absence of increase in the ionization energy or change in the crystal structure with increasing layer count, we relate the decrease in photo-emission intensity to the emergence of a band gap just above the vacuum level, as observed in LEE reflectivity spectra. Second, we study the energy distribution of secondary electrons. We use electron beam damage to cause controlled changes in the band structure, and find a clear correlation between the evolution of the LEE spectra and the distribution of secondary electrons.

5.1 Introduction

Photoemission spectroscopy techniques are among the most prevalent tools to investigate the electronic band structure of solids. Depending on the energy of the photons, different electronic bands of the material are probed. Techniques such as X-ray photoelectron spectroscopy (XPS), extended X-ray absorption fine structure (EXAFS) or near edge X-ray absorption fine structure (NEXAFS) target the core shells while photoemission electron microscopy (PEEM) and angle-resolved photoelectron spectroscopy (ARPES) among others, probe the occupied (valence) bands. The depth probed is a function of the energy of the incident photons due to the mean free path of both the photons and the ejected photoelectrons [1], and is an important consideration in the correct interpretation of the material properties from photoemission spectroscopies. [2,3] Another important factor is the electron's initial excitation from an occupied state to an intermediate excited state above the vacuum energy, before it exits the material. Although short-lived, such states are known to play an important role in the photoemission process. Unfortunately, in most photoemission studies, there is no independent information on these intermediate states. Hence, the typical approach in the interpretation of photoemission data is to assume that the electrons are excited into a free-electron-like final state, ignoring the details of the unoccupied band structure. [4-7] Still, several authors have successfully incorporated unoccupied intermediate states (confusingly often referred to as "final states" in photoemission literature), usually from theoretical calculations and VLEED measurements, to explain photoemission data and resolve inconsistencies in band structure mapping. Some examples include $TiTe_2$ [4], single-crystal Ni(110) [5], SiC with a graphite overlayer [8], Cu [6,7], and monolayer and bilayer graphene. [9] Also, recently the lifetime of final states of photoelectrons has been experimentally measured in Ni(111), Ag(111) and Au(111), with values reaching ~100 attoseconds for some states. [10,11]

A related phenomenon is the emission of secondary electrons (SEs). SEs generated by exposure to high-energy electrons or photons are responsible for much of the damage caused in biological and organic materials [12,13], but they are also exploited in applications such as lithography to deliberately cause chemical changes in an organic resist material. Nonetheless, after decades of research, our understanding of the fundamental processes regarding the generation of SEs is limited. The energy and momentum of the primary beam

---

* This chapter has been published as "Critical role of electronic states above the vacuum level in photoelectron and secondary electron emission in few-monolayer pentacene films", A. Tebyani, R.M. Tromp, S.J. van der Molen - Phys. Rev. B 108, 045425 (2023)

electrons are transferred to the electrons in the sample via multiple scattering events, leading to a loss of information on the details of the interactions between the beam electrons and the sample electrons. The unoccupied band structure has been shown to also affect the emission of SEs [14], such as the case of graphene layers formed on SiC(0001), for which SEs show energy-dependent intensity distributions with six-fold symmetry and features ascribed to the band structure [15], or in other studies on graphite to explain the features in the SE emission spectra. [16-18]

Here, we use Low-Energy Electron Microscopy (LEEM) to study the interaction of crystalline pentacene films, one to four monolayers in thickness, with low-energy electrons (LEEs) as well as UV photons. Scattering of LEEs from the sample does not only provide real- and reciprocal- space information about the microstructure, but also yields direct information on unoccupied bands above the vacuum level and their dispersion. [19-20] Interestingly, these are exactly the states that can act as intermediates in photoemission and SE emission processes. Hence, their (un)availability directly affects the emission yield of photo-electrons and SEs.

Specifically, we connect LEEM-IV spectra (i.e. the intensity of specularly-reflected low energy electrons as a function of incident energy) to photoemission and SE spectra, performing a series of experiments within the same instrument. Our system of choice is pentacene, which can be grown and studied layer-by-layer in LEEM, in real-time. First, we focus on photoemission due to excitation by a standard Hg lamp ($h\nu = 4.9$ eV). For a series of well-defined layer thicknesses (0-4 monolayers), we correlate photoemission intensity with LEEM-IV spectra, which contain information about the unoccupied states just above the vacuum level. Additionally, we probe the yield and energy distribution of SEs from pentacene, for a series of electron beam energies. [21] Here, we deliberately use electron beam damage to create chemical, structural and electronic changes in the layers. [22] Doing this in a controlled manner allows us to correlate changes in LEEM spectra and SE energy distribution curves. Our experimental observations highlight the influence of the unoccupied states on secondary processes such as photoemission and SE emission.

5.2 Experimental Technique

A schematic of the LEEM instrument is shown in Fig. 5.1(a). A beam of 15 keV electrons is decelerated to a tuneable kinetic energy of just a few eV before interaction with the sample, due to a voltage bias of -15 kV from the objective lens to the sample. Reflected electrons are re-accelerated by the same electric field and guided to the detector after travelling through an

aberration-correcting path including electron mirror optics, forming a real-space or diffraction image on the detector screen. [23,24] A high-pressure Hg UV lamp attached to the sample chamber provides the possibility for PEEM. All measurements are carried out in ultrahigh vacuum (UHV) and at room temperature.

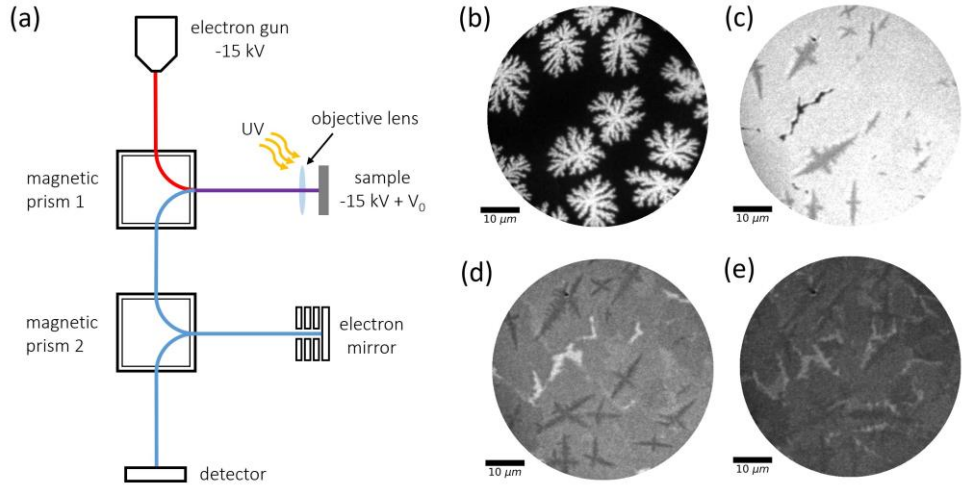

Fig. 5.1 (a) Schematic of LEEM instrument. The electron beam follows the path indicated by the red line towards the sample. The electric field between the sample and the objective lens decelerates the electrons to an energy of eV_0, tuned by setting the sample voltage. The blue line shows the trajectory of the reflected electrons toward the detector. The purple line shows where the path of the incident and the reflected beams overlap. The electron mirror corrects lower-order aberrations. Magnetic prisms separate incoming and outgoing beams and allow for electron energy spectra due to their dispersive character. In PEEM, the electron gun is turned off and the sample is irradiated with photons from a (Hg) light source. Photo-emitted electrons are subsequently imaged. (b-e) PEEM images of various stages of pentacene layer growth: (b) initial stage of nucleation and formation of the first pentacene layer in thin film phase (b) initial stage of nucleation of the second layer, which appears darker (d) initial stage of nucleation of the third layer (e) initial stage of nucleation of the fourth layer, which creates little contrast with the third layer.

5.3 Results and Discussion

The pentacene layers are grown *in situ* on silicon substrates using a Knudsen cell evaporator with line of sight to the sample. The growth dynamics of the layers is monitored in real-time both in LEEM and PEEM, as described in the literature. [25-27] At the start of sublimation, pentacene molecules are chemisorbed due to the dangling bonds on the atomically clean Si surface, leading to a decrease in photoemission intensity [27] (see Fig. S5.1 in Supporting Information Part A [28]). Afterwards, nucleation spots with higher photoemission intensity appear, which grow and merge as the sublimation continues (Fig. 5.1(b)). These nucleation spots thus evolve into the first pentacene layer in the standing-up thin-film phase. The

diffraction pattern of this layer shows that it is in a herringbone crystal structure, consistent with the literature. [25] As growth continues, subsequent layers form on top of the first layer. From the diffraction patterns of these additional layers, we find the same crystal structure as for the first layer (see Fig. S5.2 in Supporting Information Part B [28]).

Hg PEEM images capturing various stages of growth are shown in Fig. 5.1(b-e). The weak photoemission signal from the substrate is due to the higher ionization energy (IE) of silicon compared to the energy of the incoming photons (the IE being the minimum amount of energy required to extract a photoelectron from the sample). [29] As is evident from Fig. 5.1(b-e), the photoemission intensity drops for each subsequent pentacene layer after the first, even though the crystalline structure of the layers remains the same. This suggests an increase in IE with increasing layer thickness.

In the literature, the addition of consecutive layers has been reported to increase the polarization energy of a molecular layer, thereby resulting in a reduction of the ionization energy. [30] Furthermore, although ionization energies reported for the thin film pentacene phase on SiO_2 range between 4.69 eV and 4.93 eV for 1-20 nm films, no consistent dependence of IE on film thickness has been observed. [31-36] In fact, a decrease in IE of pentacene films on SiO_2 with increasing thickness in the 1-20 nm range, accompanying broadening and splitting of the HOMO band, has been reported. [35] As the PEEM intensity changes observed in Fig. 5.1(b-e) cannot be explained by these reports, another explanation is due. This prompts us to investigate the role of unoccupied states. If the unoccupied states just above the vacuum level were to change as a function of pentacene layer thickness, the photoemission yield would also become a function of thickness. In LEEM, the energy of the incident electrons can be precisely tuned by changing the sample potential. Measuring the intensity of specularly reflected electrons as a function of the incident electron energy yields an intensity-vs-voltage plot, a LEEM-IV spectrum. Such LEEM-IV spectra are largely determined by the unoccupied band structure above the vacuum level. [4,7,19,20, 37-39] At electron energies corresponding to a bandgap (zero density of unoccupied states), incoming electrons cannot enter the sample, resulting in high reflectivity. At energies corresponding to an unoccupied state (or band) in the material, the reflectivity will be low. In the latter case, the reflectivity is determined by the coupling strength of the electron plane wave (coming from the vacuum) to the unoccupied sample state, i.e. by the Schrödinger equation. Since both key parameters (unoccupied DOS *and* coupling probabilities) also affect photoemission, LEEM spectra are particularly helpful in understanding the intricacies of photoemission. [9,40]

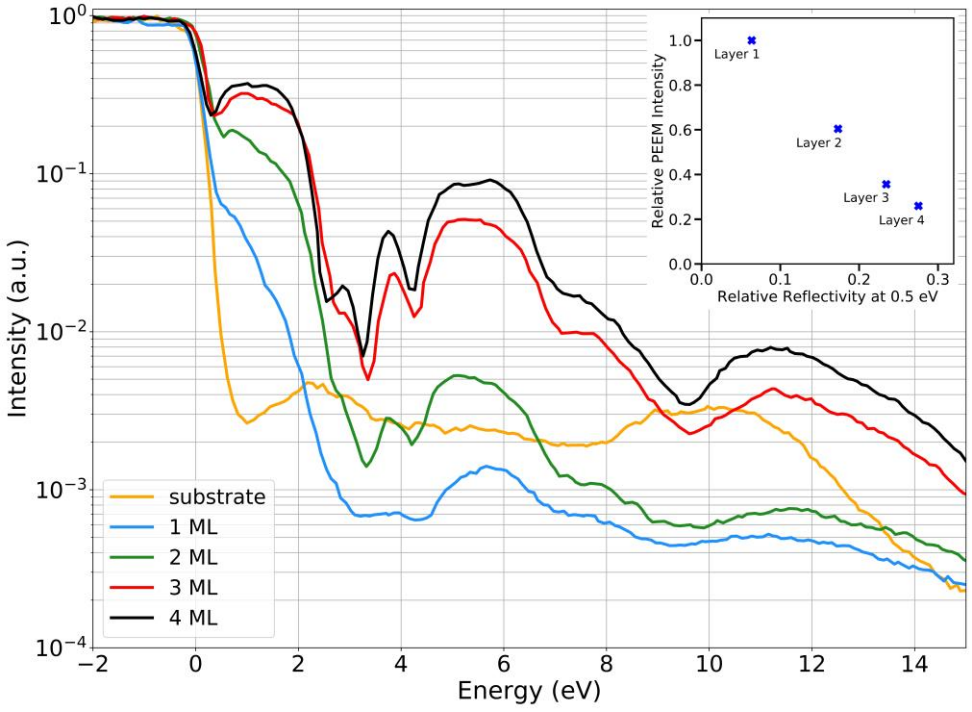

Fig. 5.2 (main) LEEM-IV spectra showing the evolution of reflectivity of a pentacene film across four layer counts. An energy of 0 eV corresponds to vacuum level. Negative energies indicate the electrons do not have enough kinetic energy to reach the sample, resulting in total reflection. The spectra for higher layer counts are more pronounced. Note the emergence of a bandgap 0-2 eV above the vacuum level as the number of layers increases. (inset) Relative PEEM intensity of various layer counts obtained from Fig. 5.1 vs. the reflectivity from LEEM-IV spectra at 0.5 eV.

In Fig. 5.2, we show LEEM-IV spectra for pentacene films of one to four monolayers in thickness, as well as for the Si substrate. Here, 0 eV corresponds to the vacuum level, and negative energies indicate insufficient kinetic energy for the incoming electrons to reach the sample (due to the negative sample bias), resulting in total reflection. The spectra in Fig. 5.2 are obtained from the same sample. The growth was paused after each subsequent layer, and several (2-6) LEEM-IV spectra were measured. Each of the spectra in Fig. 5.2 is the average of the spectra of the same layer count on the sample. The relative reflection intensity for different layer counts was consistent in all these measurements, i.e. higher layer counts resulted in higher reflection also in each of the individual measurements. The LEEM-IV spectra in Fig. 5.2, as well as the PEEM images in Fig. 5.1, were reproduced in several other samples.

The most noticeable observation in Fig. 5.2 is that the pentacene-related spectral features become more pronounced with increasing layer count. This is partly due to the better crystallinity of higher layers (as evidenced by sharper diffraction peaks) resulting in sharper spectra, and partly due to the diminishing effect of the substrate (which has generally lower reflectivity) on the measured reflectivity in thicker films, and also partly due to the developing pentacene band structure with increasing layer thickness.

The intensity in all five LEEM-IV spectra starts to drop at the same electron energy of ~0 eV, indicating an absence of any change in work function (i.e. the distance between Fermi energy and vacuum level) between films of different thicknesses. This indeed confirms previous articles reporting the work function of pentacene films on SiO_2 and ITO to exhibit almost no change for film thicknesses from 1 nm to 20 nm. [35,41] The main feature in Fig. 5.2, however, is a marked increase in reflectivity between 0 eV and 2 eV, as the film gets thicker. That is, a bandgap appears to develop in this energy range. Moreover, given the Hg photon energy and the IEs reported for the pentacene film in the literature, the photoelectrons are expected to have "final-state" energies located within this developing bandgap. Hence, for thicker films, electrons are less likely to be photo-excited, decreasing the probability of photoemission. We note that the LEEM-IV's show a smaller degree of change in reflectivity for each consecutive layer in the 0-2 eV region; i.e. whereas the difference in reflectivity between the one-monolayer and two-monolayer films is considerable, the relative difference between three-monolayer and four-monolayer films is much smaller. This observation is compatible with the slowing changes in PEEM intensities for thicker layers, see Fig. 5.1(b-e). To highlight their relation, the inset of Fig. 5.2 plots PEEM intensity vs. electron reflectivity at 0.5 eV for the different layer counts. We find a clear, negatively sloped relation. From the above, and the previous discussion on IE, we conclude that the changes observed in photoemission are directly related to changes in the unoccupied DOS just above the vacuum energy, not to changes in IE.

Next, we focus on the role of unoccupied states in secondary electron emission (resulting from impinging primary electrons). Influence of the unoccupied electronic states on the ejection of both low-energy photoelectrons and SEs can be found in the literature in the form of observed similarities between photoelectron and SE spectra. [42,43] A study of silver islands on Si(111) found Ag(111) islands to appear brighter in PEEM and also exhibit higher SE emission compared to Ag(001) islands, an observation attributed to the differences in the DOS above the vacuum level between the two. [44,45] Here, we measure and analyze LEEM-IV spectra in conjunction with SE energy spectra to provide further insight into the emission of SEs. SE energy spectra can be obtained *in situ* in LEEM, taking advantage of the energy dispersion of the magnetic prism arrays (Fig. 5.1(a)). [21]

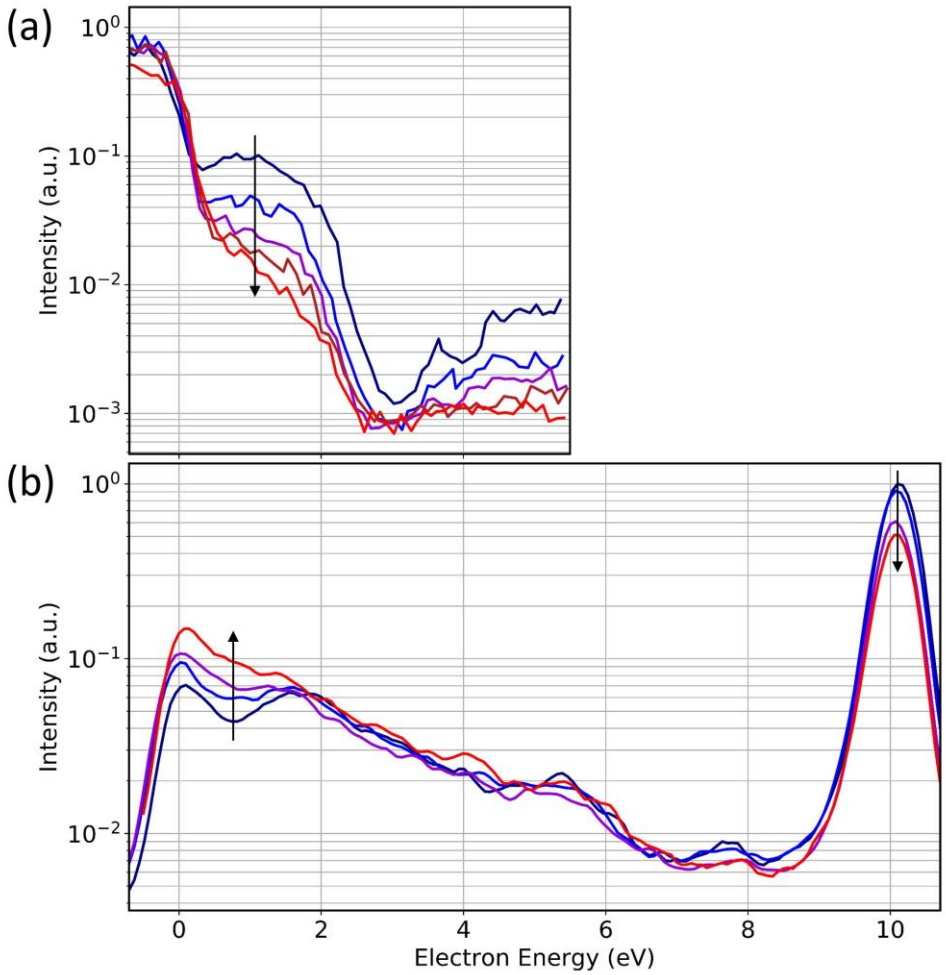

Fig. 5.3 Concomitant evolution of LEEM-IV spectra (a) and electron energy spectra (b) as a result of continued exposure to the electron beam (dark blue towards red). The pentacene film is three monolayers in thickness. (a) Changes in LEEM-IV spectra show the disappearance of the bandgap located at 0-2 eV above the vacuum energy (0 eV). (b) The dip in secondary electron distribution gradually disappears as a result of exposure to 10.1 eV electrons. (b) is measured on the same area as (a) and in between LEEM-IV measurements. The black arrows in (a) and (b) point in the direction of increased exposure to the beam. The beam current density during measurements of spectra as well as during exposure to 10.1 eV electrons was 6.72 pA/μm^2. Also, an aperture with an area of 1.15 μm^2 was placed along the beam's path in order to limit the measurements to a homogeneous area.

In a previous study [22], we reported a gradual diminishing of LEEM-IV features as a result of continued exposure of pentacene layers to an electron beam, attributed to beam damage and loss of crystalline order in the layers. Here, we use this change as an independent tool to

correlate SE emission and unoccupied states. In Fig. 5.3 (a) we show the evolution of LEEM-IV spectra as a 3-monolayer pentacene film is exposed to a beam of 10.1 eV electrons. Clear changes are observed, most notably the disappearance of the bandgap-related structure around 1 eV as damage progresses. The increased level of noise in LEEM-IV spectra in Fig. 5.3(a) compared to Fig. 5.2 is due to placement of a small aperture along the beam's path, lower beam current as well as to the spectra not being averaged. In Fig. 5.3 (b), we show a set of electron energy spectra that were measured alternatingly with the LEEM-IV spectra, on the same area. The strong peak at 10.1 eV corresponds to the intensity of the reflected primary electron beam, whereas the low-energy distribution (0-5 eV) corresponds to SEs (see also Supporting Information Part C [28]). Note the clear dip in the spectrum around 1 eV. As beam damage proceeds, the electron energy spectra exhibit both a reduction in the intensity of the elastic peak at 10.1 eV and an increase in SE emission around 1 eV (figure colors: dark blue toward red). Specifically, the dip between 0 and 2 eV disappears in the later spectra (see Fig. S5.3 in Supporting Information Part C [28] for more examples). This change in SE spectra thus happens concomitant with the diminishing of the bandgap between 0 eV and 2 eV in Fig. 5.3 (a) due to beam damage. These observations were reproduced in several other samples as well. We note that the measurements of the LEEM-IV spectra themselves (taken in-between measurements of the electron energy spectra) are expected to cause only minimal damage. This is due to the negligible damage cross-section of pentacene films for electrons of energies up to ~5.5 eV [22], i.e. the energy up to which the LEEM-IV spectra in Fig. 5.3(a) were obtained. Hence, the changes in Fig. 5.3(b) are only caused by exposure to electrons of fixed energy (10.1 eV). The exposure period varied between ~1 minute for the exposure between the first two electron energy spectra, and ~10 minutes between the last two spectra, indicating a faster rate of change in the electronic properties of the sample at the beginning, i.e. when the sample is pristine.

Our interpretation is that the states above the vacuum level play a key role in the SE spectra observed. Specifically, the bandgap at energies 0-2 eV above the vacuum energy suppresses the ejection of SEs with those energies, due to a lower density of available (intermediate) states. This results in the appearance of a dip in the energy distribution of SEs for pristine pentacene layers. The disappearance of a well-defined bandgap - as a result of chemical and electronic changes in the sample due to beam exposure - results in a higher density of available states for the SEs, hence creating a pathway for emission of SEs. This is similar to the case of photoemission discussed above. Note that previous UPS measurements on pentacene films on SiO_2 and ITO, with the same herringbone-like structure, have also reported a dip in the energy distribution of SEs. Interestingly, such a pattern was not observed in pentacene films on HOPG, where the molecules adopt a recumbent orientation. [35,41]

This marked difference led to the attribution of the SE pattern to film structure-dependent unoccupied DOS, similarly to what is discussed here.

5.4 Conclusions

Summarizing, we have highlighted the importance of the unoccupied band structure in the interpretation of data from photoemission spectroscopies and secondary electron measurements. For this, we have combined and compared direct measurements of LEEM-IV spectra above the vacuum level in thin pentacene layers, performed by LEEM, with photoemission and secondary electron energy distribution measurements. We find that knowledge of the DOS above the vacuum energy is essential for a detailed analysis of photoemission measurements. Our data also indicate that the energy distribution and yield of secondary electrons are modulated by unoccupied states above the vacuum level. Hence, this material property should also be taken into account to understand and model generation and ejection of secondary electrons. In conclusion, we have demonstrated that LEEM-IV spectra, which provide direct information on the unoccupied states, form an essential piece of information in the analysis of both photoemission and secondary electron emission processes.

References

[1] M. P. Seah and W. A. Dench, *Quantitative Electron Spectroscopy of Surfaces: A Standard Data Base for Electron Inelastic Mean Free Paths in Solids*, Surf. Interface Anal. **1**, 2 (1979).

[2] T. Wagner, G. Antczak, M. Györök, A. Sabik, A. Volokitina, F. Gołek, and P. Zeppenfeld, *Attenuation of Photoelectron Emission by a Single Organic Layer*, ACS Appl. Mater. Inter. **14**, 23983 (2022).

[3] T. Wagner, G. Antczak, E. Ghanbari, A. Navarro-Quezada, M. Györök, A. Volokitina, F. Marschner, and P. Zeppenfeld, *Standard Deviation of Microscopy Images Used as Indicator for Growth Stages*, Ultramicroscopy **233**, 113427 (2022).

[4] V. N. Strocov, E. E. Krasovskii, W. Schattke, N. Barrett, H. Berger, D. Schrupp, and R. Claessen, *Three-Dimensional Band Structure of Layered $TiTe_2$: Photoemission Final-State Effects*, Phys. Rev. B **74**, 195125 (2006).

[5] X. Y. Cui, E. E. Krasovskii, V. N. Strocov, A. Hofmann, J. Schäfer, R. Claessen, and L. Patthey, *Final-State Effects in High-Resolution Angle-Resolved Photoemission from Ni(110)*, Phys. Rev. B **81**, 245118 (2010).

[6] V. N. Strocov et al., *Absolute Band Mapping by Combined Angle-Dependent Very-Low-Energy Electron Diffraction and Photoemission: Application to Cu*, Phys. Rev. Lett. **81**, 4943 (1998).

[7] V. N. Strocov, H. I. Starnberg, and P. O. Nilsson, *Mapping the Excited-State Bands above The vacuum Level with VLEED: Principles, Results For Cu, and the Connection to Photoemission*, J. Phys.: Condens. Matter **8**, 7539 (1996).

[8] N. Barrett, E. E. Krasovskii, J. M. Themlin, and V. N. Strocov, *Elastic Scattering Effects in the Electron Mean Free Path in a Graphite Overlayer Studied by Photoelectron Spectroscopy and LEED*, Phys. Rev. B **71**, 035427 (2005).

[9] E. Krasovskii, *One-Step Theory View on Photoelectron Diffraction: Application to Graphene*, Nanomaterials **12**, 4040 (2022).

[10] Z. Tao, C. Chen, T. Szilvási, M. Keller, M. Mavrikakis, H. Kapteyn, and M. Murnane, *Direct Time-Domain Observation of Attosecond Final-State Lifetimes in Photoemission from Solids*, Science **353**, 62 (2016).

[11] R. Locher, L. Castiglioni, M. Lucchini, M. Greif, L. Gallmann, J. Osterwalder, M. Hengsberger, and U. Keller, *Energy-Dependent Photoemission Delays from Noble Metal Surfaces by Attosecond Interferometry*, Optica **2**, 2334 (2015).

[12] L. Sanche, *Low Energy Electron-Driven Damage in Biomolecules*, Eur. Phys. J. D **35**, 367 (2005).

[13] B. Boudaïffa, P. Cloutier, D. Hunting, M. A. Huels, and L. Sanche, *Resonant Formation of DNA Breaks by Low-Energy (3 to 20 eV) Electrons*, Science **287**, 1658 (2000).

[14] A. Bellissimo, G. M. Pierantozzi, A. Ruocco, G. Stefani, O. Y. Ridzel, V. Astašauskas, W. S. M. Werner, and M. Taborelli, *Secondary Electron Generation Mechanisms in Carbon Allotropes at Low Impact Electron Energies*, J. Electron Spectrosc. **241**, 146883 (2020).

[15] H. Hibino, H. Kageshima, F. Z. Guo, F. Maeda, M. Kotsugi, and Y. Watanabe, *Two-Dimensional Emission Patterns of Secondary Electrons from Graphene Layers Formed on SiC(0 0 0 1)*, Appl. Surf. Sci. **254**, 7596 (2008).

[16] F. Maeda, T. Takahashi, H. Ohsawa, S. Suzuki, H. Suematsu, *Unoccupied-Electronic-Band Structure of Graphite Studied by Angle-Resolved Secondary-Electron Emission and Inverse Photoemission*, Phys. Rev. B **37**, 4482 (1988).

[17] K. Ueno, T. Kumihashi, K. Saiki, and A. Koma, *Characteristic Secondary Electron Emission from Graphite and Glassy Carbon Surfaces*, Jpn. J. Appl. Phys. **27**, L759 (1988).

[18] W. S. M. Werner, V. Astašauskas, P. Ziegler, A. Bellissimo, G. Stefani, L. Linhart, and F. Libisch, *Secondary Electron Emission by Plasmon-Induced Symmetry Breaking in Highly Oriented Pyrolytic Graphite*, Phys. Rev. Lett. **125**, 196603 (2020).

[19] J. Jobst, A. J. H. van der Torren, E. E. Krasovskii, J. Balgley, C. R. Dean, R. M. Tromp, and S. J. van der Molen, *Quantifying Electronic Band Interactions in van der Waals Materials Using Angle-Resolved Reflected-Electron Spectroscopy*, Nat. Commun. **7**, 13621 (2016).

[20] J. Jobst, J. Kautz, D. Geelen, R. M. Tromp, and S. J. van der Molen, *Nanoscale Measurements of Unoccupied Band Dispersion in Few-Layer Graphene*, Nat. Commun. **6**, 8926 (2015).

[21] R. M. Tromp, Y. Fujikawa, J. B. Hannon, A. W. Ellis, A. Berghaus, and O. Schaff, *A Simple Energy Filter for Low Energy Electron Microscopy/Photoelectron Emission Microscopy Instruments*, J. Phys. - Condens. Mat. **21**, 314007 (2009).

[22] A. Tebyani, F. B. Baalbergen, R. M. Tromp, and S. J. van der Molen, *Low-Energy Electron Irradiation Damage in Few-Monolayer Pentacene Films*, J. Phys. Chem. C **125**, 26150 (2021).

[23] S. M. Schramm, J. Kautz, A. Berghaus, O. Schaff, R. M. Tromp, and S. J. van der Molen, *Low-Energy Electron Microscopy and Spectroscopy with ESCHER: Status and Prospects*, IBM J. Res. Dev. **55**, 1:1 (2011).

[24] R. M. Tromp, J. B. Hannon, A. W. Ellis, W. Wan, A. Berghaus, and O. Schaff, *A New Aberration-Corrected, Energy-Filtered LEEM/PEEM Instrument. I. Principles and Design*, Ultramicroscopy **110**, 852 (2010).

[25] A. Al-Mahboob, J. T. Sadowski, Y. Fujikawa, K. Nakajima, and T. Sakurai, *Kinetics-Driven Anisotropic Growth of Pentacene Thin Films*, Phys. Rev. B **77**, 035426 (2008).

[26] F. J. Meyer zu Heringdorf, M. C. Reuter, and R. M. Tromp, *The Nucleation of Pentacene Thin Films*, Appl. Phys. A **78**, 787 (2004).

[27] Frank-J. Meyer zu Heringdorf, M. C. Reuter, and R. M. Tromp, *Growth Dynamics of Pentacene Thin Films*, Nature **412**, 517 (2001).

[28] See Supporting Information for PEEM during initial stage of sublimation, diffraction pattern of pentacene thin film phase and secondary electron Energy Spectra.

[29] C. Sgiarovello, N. Binggeli, and A. Baldereschi, *Influence of Surface Morphology on the Si(100) and (111) Ionization Potentials*, Phys. Rev. B **64**, 195305 (2001).

[30] S. M. Ryno, C. Risko, and J. L. Brédas, *Impact of Molecular Orientation and Packing Density on Electronic Polarization in the Bulk and at Surfaces of Organic Semiconductors*, ACS Appl. Mater. Inter. **8**, 14053 (2016).

[31] F. Bussolotti, S. Kera, K. Kudo, A. Kahn, and N. Ueno, *Gap States in Pentacene Thin Film Induced by Inert Gas Exposure*, Phys. Rev. Lett. **110**, 267602 (2013).

[32] I. Salzmann et al., *Intermolecular Hybridization Governs Molecular Electrical Doping*, Phys. Rev. Lett. **108**, 035502 (2012).

[33] Y. M. Lee, J. W. Kim, H. Min, T. G. Lee, and Y. Park, *Growth Morphology and Energy Level Alignment of Pentacene Films on SiO_2 Surface Treated with Self-Assembled Monolayer*, Curr. Appl. Phys. **11**, 1168 (2011).

[34] S. Duhm, I. Salzmann, G. Heimel, M. Oehzelt, A. Haase, R. L. Johnson, J. P. Rabe, and N. Koch, *Controlling Energy Level Offsets in Organic/Organic Heterostructures Using Intramolecular Polar Bonds*, Appl. Phys. Lett. **94**, 033304 (2009).

[35] H. Fukagawa, H. Yamane, T. Kataoka, S. Kera, M. Nakamura, K. Kudo, and N. Ueno, *Origin of the Highest Occupied Band Position in Pentacene Films from Ultraviolet Photoelectron Spectroscopy: Hole Stabilization versus Band Dispersion*, Phys. Rev. B **73**, 245310 (2006).

[36] H. Fukagawa, S. Kera, T. Kataoka, S. Hosoumi, Y. Watanabe, K. Kudo, and N. Ueno, *The Role of the Ionization Potential in Vacuum-Level Alignment at Organic Semiconductor Interfaces*, Adv. Mater. **19**, 665 (2007).

[37] E. Bauer, *Surface Microscopy with Low Energy Electrons* (Springer New York, NY, 2014)

[38] J. B. Pendry, *The Application of Pseudopotentials to Low-Energy Electron Diffraction II: Calculation of the Reflected Intensities*, J. Phys. C: Solid State Phys. **2**, 2273 (1969).

[39] J. B. Pendry, *Theory of Photoemission*, Surf. Sci. **57**, 679 (1976).

[40] J. I. Flege and E. E. Krasovskii, *Intensity-Voltage Low-Energy Electron Microscopy for Functional Materials Characterization*, Phys. Status Solidi **8**, 463 (2014).

[41] W. Han, H. Yoshida, N. Ueno, and S. Kera, *Electron Affinity of Pentacene Thin Film Studied by Radiation-Damage Free Inverse Photoemission Spectroscopy*, Appl. Phys. Lett. **103**, 123303 (2013).

[42] N. Ueno, S. Kiyono, and T. Watanabe, *Electron Scattering from Pentacene and Coronene Polycrystals*, Chem. Phys. Lett. **46**, 89 (1977).

[43] K. Seki, T. Hirooka, Y. Kamura, and H. Inokuchi, *Photoemission from Polycyclic Aromatic Crystals in the Vacuum-Ultraviolet Region. V. Photoelectron Spectroscopy by the Rare Gas Resonance Lines and Vacuum-Ultraviolet Absorption Spectra*, B. Chem. Soc. Jpn. **49**, 904 (1976).

[44] Y. Fujikawa, T. Sakurai, and R. M. Tromp, *Surface Plasmon Microscopy Using an Energy-Filtered Low Energy Electron Microscope*, Phys. Rev. Lett. **100**, 126803 (2008).

[45] Y. Fujikawa, T. Sakurai, and R. M. Tromp, *Micrometer-Scale Band Mapping of Single Silver Islands in Real and Reciprocal Space*, Phys. Rev. B **79**, 121401(R) (2009).

Supporting Information

Part A: PEEM during initial stage of sublimation

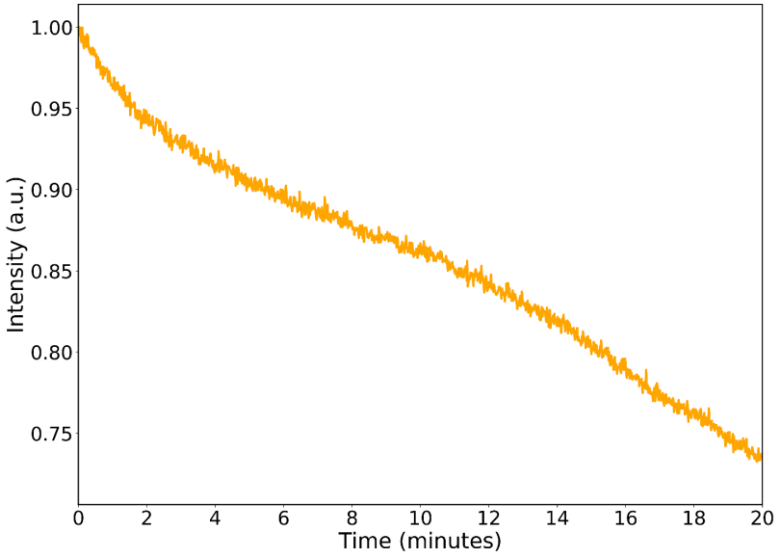

Fig. S5.1 Change in PEEM intensity during the initial stage of sublimation of pentacene on silicon (chemisorption stage), before nucleation spots of the standing-up thin-film phase appear

Part B: Diffraction pattern of pentacene thin film phase

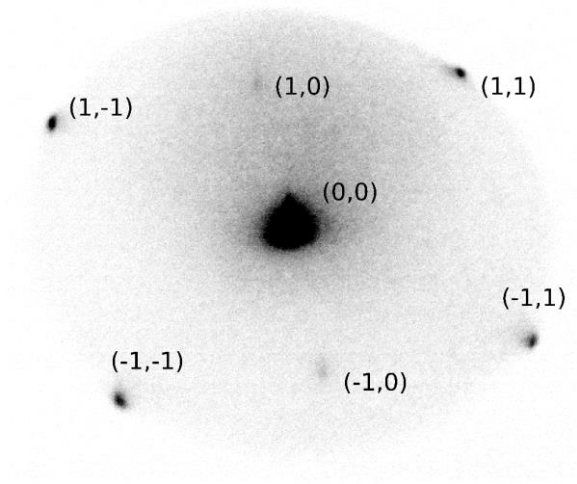

Fig. S5.2 Diffraction pattern corresponding to the standing-up thin-film pentacene phase with herringbone crystal structure, obtained from a film with four monolayers in thickness

Part C: Secondary Electron Energy Spectra

Fig. S5.3 shows energy spectra obtained for a pentacene film, four monolayers in thickness, for a series of incident electron beam energies. There are two curves for each incident beam energy. The first corresponds to the pristine area (black curves), while the second curve (orange) refers to the same area after a period of exposure to the beam, causing intentional beam damage. The strong peak at the right in all the spectra corresponds to the intensity of the elastically reflected electron beam. The distribution at the left corresponds to secondary electrons (SEs), which have kinetic energies of mostly 0-5 eV. Any peaks in between these ranges are due to inelastic scattering causing excitations in the sample, and as a result occur at specific material-dependent energies with respect to the primary beam, although their intensities are in general a function of the primary beam energy. For pentacene layers, the first five energy loss peaks are reported to occur at 2.15 eV, 4.29 eV, 5.68 eV, 6.81 eV and 8.16 eV lower energies compared to the primary beam. [1] The first two of these peaks are indicated in Fig. S5.3 by blue and green lines, respectively. As expected for peaks caused by specific, identifiable excitations in the pentacene layer, these peaks track with the peak associated with the elastically reflected electrons. The two spectra in each subfigure of Fig. S5.3 are normalized to the same value (maximum of the black curve).

Examining the energy distribution of the SEs of pristine areas, i.e. the black curves in Fig. S5.3, we notice the same pattern in all of them: a clear dip in intensity is seen between 0 and 2 eV, independent of the incident electron beam energy (black lines). After prolonged electron beam exposure, this dip is seen to disappear (orange lines), similar to what is seen in Fig. 5.3(b).

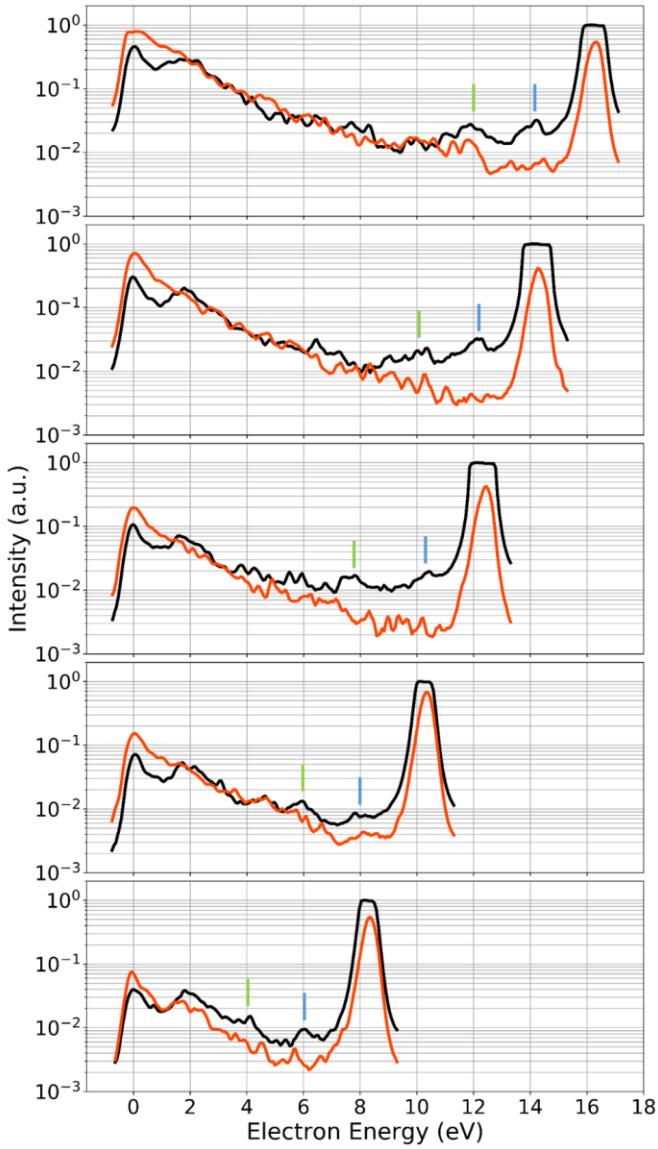

Fig. S5.3 Electron Energy Spectra of a four-monolayer pentacene film before (black) and after (orange) electron-beam irradiation, obtained for various incident energies of the electron beam. In each curve, the strong peak at the right corresponds to the primary beam intensity, which has an energy of 16.3 eV, 14.3 eV, 12.3 eV, 10.3 eV and 8.3 eV for the subfigures from the top toward the bottom, respectively. The distribution at low energies corresponds to the secondary electrons. Any peaks in between are a result of inelastic scattering causing crystal excitations. Two of such excitations are indicated in each plot by blue and green lines. The secondary electron energy distribution of all the spectra before irradiation (black) show a pattern of two peaks at 0 eV (vacuum level) and ~2 eV, separated by a dip. The same pattern is observed irrespective of the incident beam energy indicating that the peaks are not caused by inelastic scattering causing crystal excitations. This dip is virtually gone after irradiation (orange curves). See also Fig. 5.3(b).

References

[1] N. Ueno, S. Kiyono, and T. Watanabe, *Electron Scattering from Pentacene and Coronene Polycrystals*, Chem. Phys. Lett. **46**, 89 (1977).